2009 American Control Conference
Hyatt Regency Riverfront, St. Louis, MO, USA
June 10-12, 2009

Bifurcation Analysis of a Thalamic Relay Neuron Model

Huibing Yin, Charles L. Cox, Prashant G. Mehta and Uday V. Shanbhag

Abstract— **Thalamus is concerned with the *relay* of visual information from the retina to the visual cortex. Interestingly, the information transfer is strongly mediated by nonlinear dynamics of the neurons. In particular, experiments have shown that the thalamic neurons process visual input in two distinct nonlinear dynamic modes, the so-called tonic mode and the burst mode. This paper is concerned with a bifurcation analysis of the Hodgkin-Huxley type models of thalamic neurons. The analysis is used to show that the tonic mode arises as a type of global bifurcation where a homoclinic orbit interacts with a saddle node bifurcation in equilibria. Such a bifurcation is very efficient at the kind of rate coding that has been experimentally observed in the tonic mode. The burst mode is consistent with a subcritical Hopf bifurcation in slow currents. Finally, for both modes, the electrophysiological role of the so-called slow and fast currents is also discussed.**

I. Introduction

The thalamus is a centrally located brain structure through which most sensory information (including visual input from retina) must pass prior to transfer to the neocortex. At this level, the thalamic circuit integrates signals from the retina, feedback signals from the neocortex, and arousal/attention-related signals from the brainstem [1]. Although the role of the thalamus in sensory and visual signal processing is appreciated, the fundamental aspects of its *function* are not understood [2].

From an input-output standpoint, the thalamic circuit relays retinal input to thalamic output (into cortex) and as such represents an early stage of visual signal processing. Experimental studies indicate that there are two modes of information transfer in a thalamic circuit: the tonic mode and the burst mode [3]. Figure 1 depicts the experimentally obtained action potential discharge for neurons in these two modes [3].

In this paper, we investigate the role of nonlinear dynamics underlying the transfer of information in these two modes. There is a rich literature that shows that the nonlinear dynamics are important in mediating information flow in neurons (e.g., [4], [5], [6]). The study is carried out with the aid of a model of a thalamocortical (TC) relay neuron in the dorsal lateral geniculate nucleus (dLGN) in thalamus. The Hodgkin-Huxley model of the TC neuron includes single compartment models of fast sodium (Na^+) and potassium (K^+) currents, and the slow low-threshold calcium (Ca^{2+}) and hyperpolarization-activated sag currents. Time-domain simulations with the model show equilibrium, burst and tonic responses as the input current I_{in} is varied. The input current models a generic input to the TC neuron (for e.g., an input from ganglion cells in the retina).

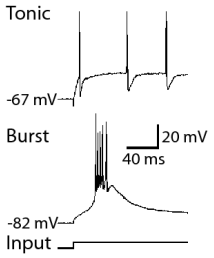

Fig. 1. Experimentally observed tonic and burst modes [3].

To better understand the observed responses, we carry out a systematic bifurcation study with the input current I_{in} serving as a continuation parameter. To get a handle on the relative influence of the slow and fast currents, the study is first carried out for models where either the slow or the fast current is turned off. For example, the slow current is turned off by setting the value of conductances for the low-threshold calcium and hyperpolarization-activated sag currents equal to zero. Such a study is used to show that the slow currents have a rather small effect on the tonic mode response characteristics.

The bifurcation analysis helps explain the nonlinear dynamics underlying the two modes. In particular, the analysis is used to show that the tonic mode arises as a result of the saddle node on invariant circle (SNIC) [4] bifurcation. It refers to a type of global bifurcation where a homoclinic orbit interacts with a saddle node bifurcation in equilibria [4]. The bifurcation is very efficient at the kind of rate coding that has been experimentally observed in the tonic mode. The burst mode is shown to be consistent with a subcritical Hopf bifurcation in slow currents. Such a bifurcation helps explain the observed slow frequency characteristics of the burst mode.

The remainder of the paper is organized as follows. Section II presents the details of modeling a TC neuron and section III describes the results of time-domain simulations as the input current I_{in} is varied. Section IV presents the results of continuation study carried out with the input current I_{in} as the free parameter with the aid of software AUTO. The bifurcation diagram together with nonlinear dynamics underlying the rate coding in tonic mode are described in detail. The conclusions and some directions for

H. Yin and P. G. Mehta are with the Coordinated Science laboratory and the Department of Mechanical Science and Engineering at the University of Illinois at Urbana-Champaign (UIUC), 1206 W. Green Street, Urbana, IL 61801. yin3@illinois.edu; mehtapg@illinois.edu

C. L. Cox is with the Department of Molecular and Integrative Physiology at UIUC cox2@illinois.edu

U. V. Shanbhag is with the Department of Industrial and Enterprise Systems Engineering at UIUC udaybag@illinois.edu

978-1-4244-4524-0/09/$25.00 ©2009 AACC

future research are discussed in Section V.

II. Modeling

We consider a conductance-based single compartment model ([7], [8], [4]) of a single TC neuron:

$$C\frac{\mathrm{d}V}{\mathrm{d}t} = I_{\text{in}} - I_{\text{mem}}, \tag{1}$$

where C is the capacitance, V is the voltage across the membrane (also called membrane potential), I_{in} is the input current, and I_{mem} is the sum of the neuron membrane currents:

$$I_{\text{mem}} = I_L + I_T + I_h + I_{Na} + I_K.$$

It contains both passive currents and active currents. For the passive currents, we consider the potassium leakage current and the non-specific leakage current:

$$\begin{aligned} I_L &= I_{KL} + I_{NL} \\ &= g_{KL}(V - E_K) + g_{NL}(V - E_{NL}), \end{aligned}$$

where g_{KL} and g_{NL} are the potassium leakage conductance and non-specific leakage conductance, respectively, and E_K and E_{NL} are their respective reversal potentials.

For the active currents, we consider both slow and fast currents. The models for these currents are described next.

A. Slow Currents

For slow currents, we consider the T-type calcium current I_T and the hyperpolarization-activated sag current I_h:

$$\begin{aligned} I_T &= \bar{g}_T \cdot m_\infty^2(V) \cdot h \cdot (V - E_T), \\ I_h &= \bar{g}_h \cdot r \cdot (V - E_h), \end{aligned}$$

where $\bar{g}_T$ and $\bar{g}_h$ are the maximal conductances, E_T and E_h are the reversal potentials, and h and r are the gating variables for T-type calcium and sag currents, respectively. I_T has another gating variable m, which is fast compared to h. So, we replace m with its equilibrium function $m_\infty(V)$ to reduce the number of states. The dynamics of gating variables for slow currents have the generic form:

$$\frac{\mathrm{d}x}{\mathrm{d}t} = \frac{x_\infty(V) - x}{\tau_x(V)},\ x \in \{h, r\}, \tag{2}$$

where $x_\infty(V)$ is the equilibrium function of the corresponding gating variable, and $\tau_x(V)$ is the voltage-dependent time constant. The explicit formula for these appear in the appendix.

B. Fast Currents

For fast currents, we consider the fast sodium current I_{Na}, and the fast potassium current I_K:

$$\begin{aligned} I_{Na} &= \bar{g}_{Na} \cdot m_{Na,\infty}^3(V) \cdot h_{Na} \cdot (V - E_{Na}), \\ I_K &= \bar{g}_K \cdot n^4 \cdot (V - E_K), \end{aligned}$$

where $\bar{g}_{Na}$ and $\bar{g}_K$ are the maximal conductances, E_{Na} and E_K are the reversal potentials, $m_{Na,\infty}(V)$ is the equilibrium function of gating variable. h_{Na} and n are the gating variables and have the same form of dynamics as (2) with $x \in \{h_{Na}, n\}$. The explicit formula for these together with the parameter values are given in the appendix.

C. Summary of model

The model including both slow and fast currents is described by the following set of ODEs:

$$\begin{aligned} C\frac{\mathrm{d}V}{\mathrm{d}t} = I_{\text{in}} &- \overbrace{\left(g_{KL}(V - E_K) + g_{NL}(V - E_{NL})\right)}^{I_L} \\ &- \overbrace{\bar{g}_T m_\infty^2(V) \cdot h \cdot (V - E_T)}^{I_T} - \overbrace{\bar{g}_h \cdot r \cdot (V - E_h)}^{I_h} \\ &- \overbrace{\bar{g}_{Na} m_{Na,\infty}^3(V) h_{Na} (V - E_{Na})}^{I_{Na}} - \overbrace{\bar{g}_K \cdot n^4 \cdot (V - E_K)}^{I_K}, \end{aligned} \tag{3}$$

$$(slow) \quad \begin{cases} \dfrac{\mathrm{d}h}{\mathrm{d}t} &= \dfrac{h_\infty(V) - h}{\tau_h(V)}, \\ \dfrac{\mathrm{d}r}{\mathrm{d}t} &= \dfrac{r_\infty(V) - r}{\tau_r(V)}, \end{cases} \tag{4}$$

$$(fast) \quad \begin{cases} \dfrac{\mathrm{d}h_{Na}}{\mathrm{d}t} &= \dfrac{h_{Na,\infty}(V) - h_{Na}}{\tau_{h_{Na}}(V)}, \\ \dfrac{\mathrm{d}n}{\mathrm{d}t} &= \dfrac{n_\infty(V) - n}{\tau_n(V)}. \end{cases} \tag{5}$$

To model only the effect of fast currents, we set $\bar{g}_T = \bar{g}_h = 0$. This leads to a 3-state model (3) and (5) in state (V, h_{Na}, n). Similarly, the effect of slow currents alone is modeled by setting $\bar{g}_{Na} = \bar{g}_K = 0$. This leads to a 3-state model (3) and (4) in states (V, h, r).

III. Time domain simulations

In this section, we present the results of time domain simulations with the 5-state model (3)-(5); the parameter values are given in table I in the appendix. With certain negative (hyperpolarizing) constant input currents, the model exhibits a slow periodic burst with fast spikes sitting at the crest, known as burst mode. With other positive (depolarizing) constant input currents, it exhibits periodic fast spikes, known as tonic mode. The two responses are summarized next:

Burst Mode: Figure 2 (a) depicts the time-series of the response with a constant input current at the value of $I_{\text{in}} = -0.7\mu A/cm^2$. The initial membrane potential is set to $V_0 = -60\,mV$. The response shows that the slow-gating variables have the same period of rhythmicity as the burst, while the fast-gating variables have the same characteristics as the spikes of the burst. This is qualitatively consistent with the experimental results of [9], where the so-called low threshold spiking (LTS) is mainly the result of I_T and I_h [10].

Tonic Mode: Figure 2 (b) depicts the time-series of the response with a constant input current at the value of $I_{\text{in}} = 1.0\mu A/cm^2$. The initial membrane potential is set the same value as burst mode. The response shows that the value of slow-gating variables are small while the fast-gating variables dominate and have the same characteristics as the membrane potential.

To better understand the sensitivity of these two response models to system parameters, we also carried out numerical investigations with different values of g_{KL}. This parameter is thought to play an important role in regulation of response mode by brainstem [11]. Figure 2 (c) summarizes the solution regions together with the boundaries between

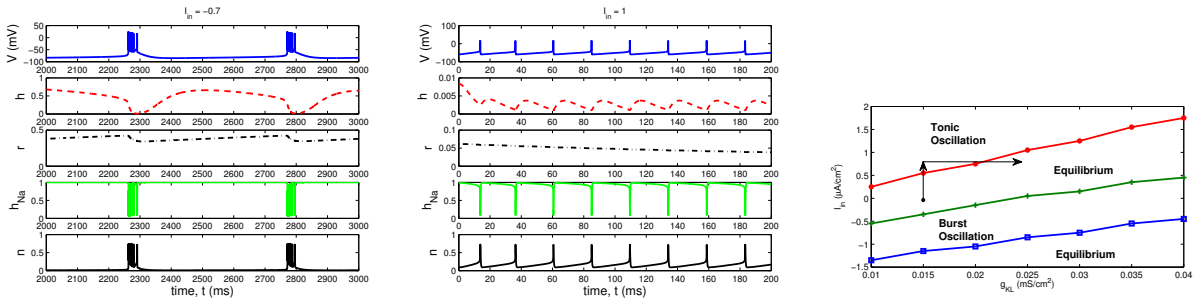

(a) (b) (c)

Fig. 2. Simulation results: (a) Burst mode; (b) Tonic mode; (c) Bifurcation diagram in (g_{KL}, I_{in}) plane.

equilibrium, burst and tonic mode for changing values of g_{KL}. In each of these regions, the time-domain simulations exhibit the stated asymptotic solution state after a brief period of transients. For a fixed value of g_{KL}, the qualitative picture of transition is same as the one just described. Quantitatively, the onset of the tonic mode requires greater threshold of input current I_{in} as g_{KL} increases.

Variations in g_{KL} can thus lead to qualitative changes in response with same input current I_{in}. For example, when $I_{\text{in}} = 0\mu A/cm^2$ and $g_{KL} = 0.015mS/cm^2$, the neuron is at an equilibrium. Suppose the input current changes suddenly to $I_{\text{in}} = 0.75\mu A/cm^2$ as a result of change in the environment, the solution transits to tonic oscillation. Similarly, for a larger value of g_{KL}, e.g. $0.025mS/cm^2$, one obtains an equilibrium solution again, as is shown by the arrows in Figure 2 (c).

IV. Bifurcation Analysis

In this section, we present the results of bifurcation analysis with the models. The analysis is carried out with the aid of continuation software AUTO [12]. The analysis is structured such that we present the results with 3-state models (slow-currents only in section IV-A and fast currents only in section IV-B) before describing results with the 5-state model in section IV-C.

A. Analysis of model with slow currents ($\bar{g}_{Na} = \bar{g}_K = 0$)

We set $\bar{g}_{Na} = \bar{g}_K = 0$ so the membrane current

$$I_{\text{mem}} = I_L + I_T + I_h.$$

The model is described by equation (3) for membrane potential and equation (4) for the two slow-gating variables h and r. In the following, we describe results of equilibrium analysis and continuation study in input current I_{in}.

The equilibria of the 3-state model are obtained by setting the right hand side of (3) and (4) to zero:

$$I_{\text{in}} - I_{\text{mem}} = 0 \tag{6}$$
$$x_\infty(V) - x = 0 \quad x \in \{h, r\}. \tag{7}$$

At the equilibrium, we have $h = h_\infty(V)$ and $r = r_\infty(V)$. Substituting these into (6), we obtain an equation only in terms of V. With three variables we have

$$\begin{aligned} F^{(s)}(V) &\doteq I_{\text{in}} - I_L - I_T - I_h \\ &= I_{\text{in}} - I_L - \bar{g}_T \cdot m_\infty^2(V) \cdot h_\infty(V) \cdot (V - E_T) \\ &\quad - \bar{g}_h \cdot r_\infty(V) \cdot (V - E_h). \end{aligned} \tag{8}$$

As a result, the equilibria of (6)-(7) are completely described in terms of equilibria of (8).

Figure 3(a) depicts the graph of function $F^{(s)}(V)$ with slow currents only. The function is monotone and there is only one equilibrium irrespective of the value of input current I_{in}. Figure 3(b) depicts the continuation of the equilibrium as I_{in} is varied. The equilibrium was found to be unstable for input current in the interval $[-1.064, -0.165](\mu A/cm^2)$. At the value of $I_{\text{in}} = -0.165$, there is a sub-critical Hopf bifurcation resulting in large amplitude oscillation. The resulting branch of periodic orbit is depicted in the figure. Each point along the periodic orbit branch depicts the maximum value of the membrane potential solution $V(t)$. The time-period of these oscillation is used to obtain the frequency that is depicted in Figure 3(c). The low frequency $(1 - 4Hz)$ nature of the solution is quantitatively consistent with the time-domain simulation (these comparisons are given in the figure) and also qualitatively consistent with the experimental results (see [10]).

B. Analysis of model with fast currents ($\bar{g}_T = \bar{g}_h = 0$)

We set $\bar{g}_T = \bar{g}_h = 0$ so the membrane current

$$I_{\text{mem}} = I_L + I_{Na} + I_K.$$

As before, the equilibria of the resulting 3-state model (3) and (5) are completely characterized by the equilibria of the function

$$\begin{aligned} F^{(f)}(V) &\doteq I_{\text{in}} - I_L - I_{Na} - I_K \\ &= I_{\text{in}} - I_L - \bar{g}_{Na} \cdot m_{Na,\infty}^3(V) \cdot h_{Na,\infty}(V) \cdot (V - E_{Na}) \\ &\quad - \bar{g}_K \cdot n_\infty^4 \cdot (V - E_K). \end{aligned}$$

This function is qualitatively different from $F^{(s)}(V)$. The fast current model has three equilibria for a certain range of input currents (see Fig. 3(d)). In the continuation space with I_{in}, the equilibrium solution branch now arises as a S-shaped curve (see Fig. 3(e)). Locally, two equilibria "disappear"

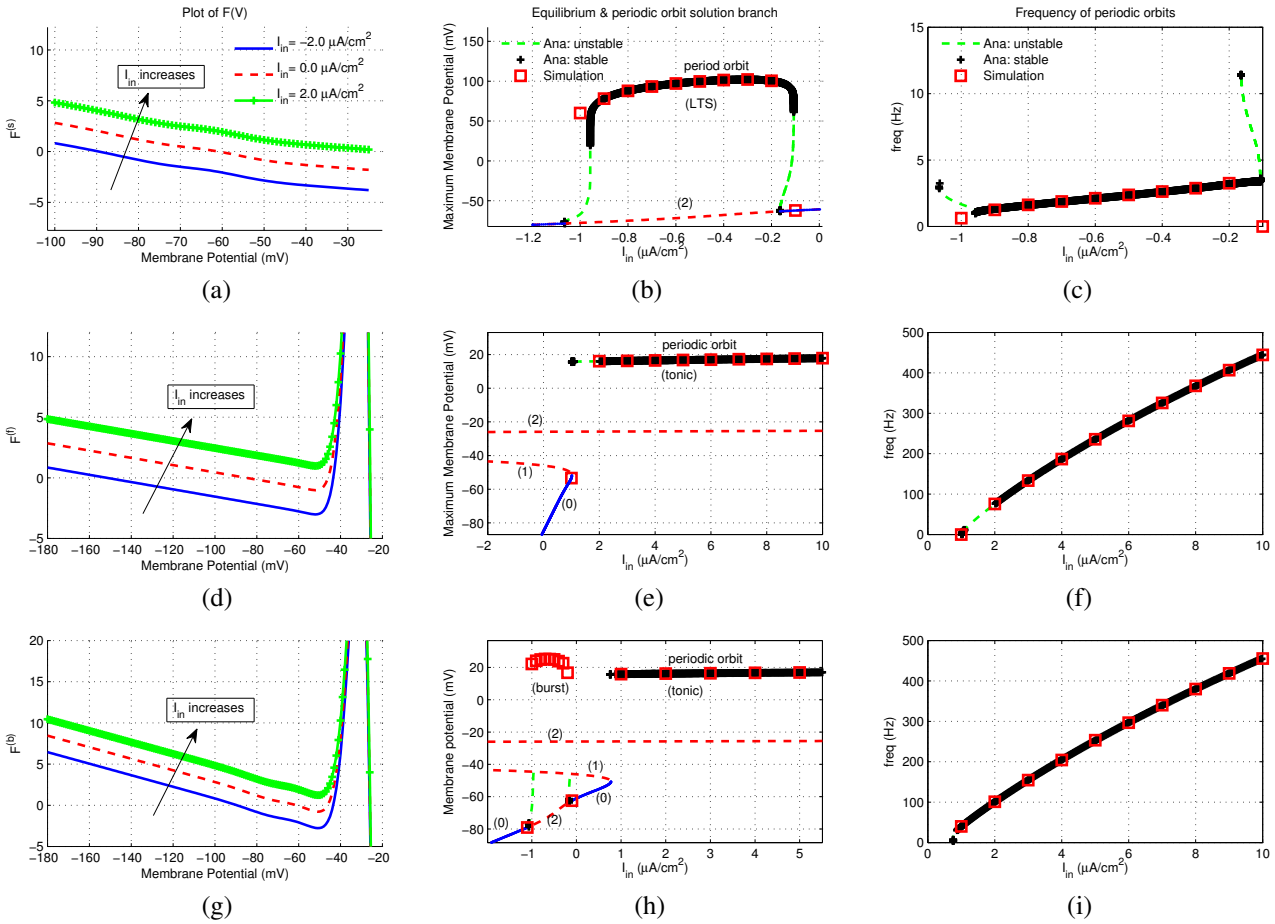

Fig. 3. Bifurcation analysis for TC model: First row (a,b,c) shows the results for slow current case; Second row (d,e,f) shows the results for fast currents; Third row (g,h,i) shows the results for both currents; First column (a,d,g) shows $F(V)$; Second column (b,e,h) shows the bifurcation diagram (blue line and red dashes indicate the equilibrium, others for periodic orbit; dashed line indicates unstable equilibrium (or periodic orbit) solutions, the number on top of dashed line indicates the number of unstable eigenvalues (Lyapunov exponents)); Third column (c,f,i) shows the frequency as a function of input current I_{in}.

via a saddle node bifurcation at the two turning points on this branch. At the lower turning point along the S-shaped branch, the equilibrium solution loses stability because a real eigenvalue crosses the imaginary axis. At the upper turning point, another eigenvalue crosses the imaginary axis into right half plane (RHP). So, the upper branch of the equilibrium solution is unstable with two eigenvalues in the RHP. For a very large value of I_{in}, the two eigenvalues in the RHP cross back into the left half plane (LHP) via a supercritical Hopf bifurcation. Continuation of the periodic orbit in I_{in} from the Hopf bifurcation point results in a branch of periodic orbit solution that are depicted in Figure 3(e) as a thick black line composed of "+". The solution terminates into a homoclinic orbit at the value of $I_{\text{in}}^{\text{c}} = 1.0\mu A/cm^2$, same as the critical value where the saddle node bifurcation occurs (lower turning point).

The phase space schematic of the resulting global bifurcation is described in Figure 4. For $I_{\text{in}} < I_{\text{in}}^{\text{c}}$, there are three equilibria, one of which is stable and other two are unstable. Time domain simulations show that the trajectories asymptote to the stable equilibrium. At $I_{\text{in}} > I_{\text{in}}^{\text{c}}$ there is only unstable equilibrium and trajectories asymptote to a stable

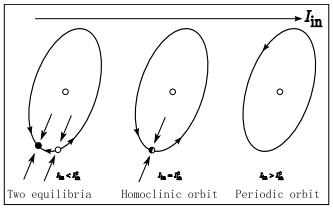

Fig. 4. Phase space schematic of the global bifurcation underlying the tonic mode: black circle indicates stable equilibrium while white circle indicates unstable one.

periodic orbit. As $I_{\text{in}} \downarrow I_{\text{in}}^{\text{c}}$ from above, the time period of the oscillation grows and at the critical point $I_{\text{in}} = I_{\text{in}}^{\text{c}}$, the orbits terminate in a homoclinic orbit. As $I_{\text{in}} \uparrow I_{\text{in}}^{\text{c}}$ from below, the two equilibria along the lower and middle branches in the S-shaped branch merge into a single marginally stable equilibrium. The homoclinic orbit represents the unstable manifold for this equilibrium. As I_{in} increases, the equilibrium disappears due to the saddle node bifurcation and the homoclinic orbit is replaced by a stable periodic orbit with a finite period.

The resulting bifurcation has an exquisite frequency cod-

ing characteristics as shown in Figure 3(f). As I_{in} increaseas beyond I_{in}^{c}, the frequency increases in a nearly linear fashion for a certain range of input current values.

C. Analysis of model with both currents

In this subsection, we present the results of bifurcation analysis with the 5-state model ((3)-(5)) that has both slow and fast currents. We begin by describing the equilibria that now are characterized by the equilibria of the function

$$\begin{aligned} F^{(b)}(V) &\doteq I_{\text{in}} - I_L - I_T - I_h - I_K - I_{Na} \\ &= I_{\text{in}} - I_L - \bar{g}_T \cdot m_\infty^2(V) \cdot h_\infty(V) \cdot (V - E_T) \\ &\quad - \bar{g}_h \cdot r_\infty(V) \cdot (V - E_h) - \bar{g}_K \cdot n_\infty^4 \cdot (V - E_K) \\ &\quad - \bar{g}_{Na} \cdot m_{Na,\infty}^3(V) \cdot h_{Na,\infty}(V) \cdot (V - E_{Na}). \end{aligned}$$

This function, depicted in Figure 3(g), is qualitatively similar to $F^{(f)}(V)$ with three equilibria in a certain range of input current. Continuation in I_{in} shows a S-shaped solution branch with two turning points. Along the lower-branch, the solution loses stability in a certain interval $[-1.064, -0.165](\mu A/cm^2)$ much the same as for the 3-state model with slow currents alone (see section IV-A). The stability characteristics at two turning points are similar to the 3-state model with fast currents alone (see section IV-B).

With the 5-state model, one gets almost the same picture of the tonic mode solution characteristics as the 3-state model with fast currents (see section IV-B and Fig. 3(e) and (h)). The global bifurcation involving a local saddle node bifurcation and a global homoclinic orbit leads to efficient frequency coding even with the 5-state model. Figure 3(i) depicts the frequency characteristics. Quantitatively, this is very similar to Figure 3(f) with 3-state alone. Thus a 3 state model with fast currents alone describes the solution behavior adequately in the tonic region.

We next describes continuation study for hyperpolarizing current ($I_{\text{in}} < 0$). As already noted, the equilibrium along the lower solution branch loses stability for input current in the interval $[-1.064, -0.165](\mu A/cm^2)$. Using time-domain simulations, one obtains a burst response mode in this interval. These solutions are depicted in Figure 3(h) using the maximum value of solution $V(t)$. Using continuation, one obtains an unstable branch of periodic orbits (shown in Fig. 3(h)) that has secondary bifurcation points (**torus bifurcation**). Our conjecture is that burst mode arises as a result of one of these secondary bifurcations. We could not validate our conjecture because obtaining such solutions via continuation methods in AUTO is currently not possible.

D. Summary

Tonic mode: Figure 2 (b) describes time-domain simulations in tonic mode for 5-state model. These are explained using the bifurcation diagram in Figure 3(e) and (h). The bifurcation involves a global bifurcation as described by Figure 4. Such a bifurcation is efficient at frequency coding (see Fig. 3(f)). Analysis of 3-state and 5-state model showed that the fast currents alone captures both the qualitative bifurcation picture as well as the quantitative value of frequency.

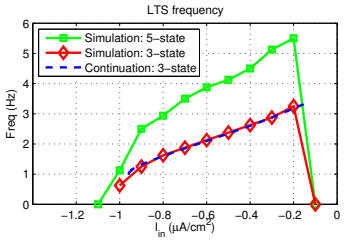

Fig. 5. Comparison of the burst response LTS frequency in time-domain simulation between 3-state and 5-state model.

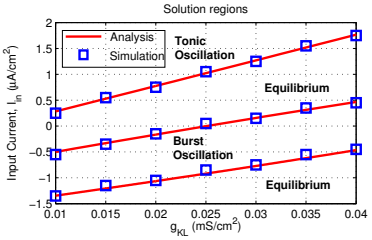

Fig. 6. Solution regions obtained using continuation and time-domain simulation.

Continuation provides an elegant alternative to obtain the periodic orbit solution in the tonic region (see Fig. 3(h)).

Burst mode: Figure 2 (a) describes time-domain simulations in burst mode for 5-state model. These simulations are partially explained using the bifurcation diagram with 3-state (slow currents only) and 5-state models. In particular, the burst arises as a result of equilibrium losing stability via Hopf bifurcation. Continuation studies with the 3-state model alone showed the slow-frequency LTS solutions. However, the time-domain simulations with 5-state model shows additional spikes due to fast currents that ride on the LTS solution (see Fig. 2 (a)). We could not use continuation to obtain this solution. Nevertheless, our studies revealed that the frequency characteristics of underlying LTS solution is qualitatively very similar for both 3-state and 5-state model (see Fig. 5). The range of currents where burst response is seen is also the same and well captured by analysis using either models. Thus, the 3-state model can be used to carry out approximate analysis of the LTS behavior underlying the burst mode solution.

Continuation with g_{KL}:

The analysis shows that the tonic response mode arises at the lower turning point (saddle node-bifurcation). We continued this point in AUTO as a function of g_{KL} to obtain the boundary for tonic mode in the (g_{KL}, I_{in}) space. Likewise, the burst mode arises due to the two Hopf bifurcation points whose continuation is used to describe the boundary for burst mode. The resulting solution region obtained using AUTO are summarized in Figure 6. Comparison with time-domain simulation is also given.

V. Conclusions and Future Work

In this paper, we carried out a systematic bifurcation analysis with Hodgkin-Huxley type models of a thalamic relay neuron. Time-domain simulations of the model show that

it exhibits different responses with different input currents. These responses were further investigated with the aid of a continuation-based study using AUTO. The analysis showed that tonic mode arises as a type of global bifurcation where a homoclinic orbit interacts with a saddle node bifurcation in equilibria. Such a bifurcation is very efficient at frequency coding. In future work, we will seek to extend this analysis to include additional neurons, such as thalamic reticular and cortical neurons. Of particular interest will be to determine the impact of inter-connections on tonic mode response characteristics.

APPENDIX

The equilibrium functions of the three gating variables m, h and r take the generic form:

$$x_\infty(V) = \frac{1}{1+e^{-(V-V_x)/k_x}},\ x \in \{m,h,r\},$$

where V_x is the value where $x_\infty(V_x) = \frac{1}{2}$ and k_x determines the slope of the curve. The positive value of k_x results in a monotonically increasing function while negative value a monotonically decreasing one. For h and n, the time constant functions are:

$$\tau_h(V) = 7.14 + \frac{52.4}{1+e^{-(V-V_{ht})/k_{ht}}},$$
$$\tau_r(V) = 20 + \frac{1000}{e^{(V-V_{rt1})/k_{rt1}} + e^{-(V-V_{rt2})/k_{rt2}}}.$$

The explicit form of fast gating variables is given by

$$x_\infty(V) = \frac{\alpha_x}{\alpha_x+\beta_x},\ x \in \{m_{Na}, h_{Na}, n\},$$
$$\tau_x(V) = \frac{1/\Phi_x}{\alpha_x+\beta_x},\ x \in \{h_{Na}, n\},$$

where Φ_x is a constant that serves to speed up the gating variable response, and α_x, β_x are the voltage dependent gating variable specific functions:

$$\alpha_{m_{Na}} = \frac{-\frac{V+29.7-\sigma_m}{10}}{e^{-(V+29.7-\sigma_m)/10}-1},$$
$$\beta_{m_{Na}} = 4e^{-\frac{V+52.7}{18}},$$
$$\alpha_{h_{Na}} = 0.07e^{-\frac{V+15.7-\sigma_{Na}}{20}},$$
$$\beta_{h_{Na}} = \frac{1}{e^{-(V-14.3-\sigma_{Na})/10}+1},$$
$$\alpha_n = \frac{-\frac{V+45.7-\sigma_K}{100}}{e^{-(V+45.7-\sigma_K)/10}},$$
$$\beta_n = 0.125e^{-\frac{V+55.7-\sigma_K}{80}}.$$

The parameters used in numerical implementation of these functions are listed in table I.

TABLE I
PARAMETER VALUES

Parameter	Value	Unit
Common		
C	1.0	$\mu F/cm^2$
Leakage current parameters		
g_{KL}	0.02	mS/cm^2
g_{NL}	0.01	mS/cm^2
E_K	−100.0	mV
E_{NL}	−55.0	mV
Slow current parameters		
g_T	2.0	mS/cm^2
g_h	0.04	mS/cm^2
E_T	120.0	mV
E_h	−40.0	mV
V_m	−59.0	mV
V_h	−81.0	mV
V_r	−75.0	mV
V_{ht}	−74.0	mV
V_{rt1}	−71.5	mV
V_{rt2}	−89.0	mV
k_m	6.2	mV
k_h	−4.4	mV
k_r	−5.5	mV
k_{ht}	−3.0	mV
k_{rt1}	14.2	mV
k_{rt2}	11.6	mV
Fast current parameters		
g_{Na}	42.0	mS/cm^2
g_K	30.0	mS/cm^2
E_{Na}	55.0	mV
σ_m	2.0	mV
σ_{Na}	−18.0	mV
σ_K	16.0	mV
Φ_{Na}	200.0/7.0	
Φ_n	200.0/7.0	

REFERENCES

[1] S. M. Sherman and R. Guillery, *Exploring the Thalamus and Its Role in Cortical Function*. Cambridge, MA: Academic Press, 2006.

[2] J. L. van Hemmen and T. J. Sejnowski, Eds., *23 problems in systems neuroscience*, ser. Computational Neuroscience (New York). New York: Oxford University Press, 2006.

[3] S. Lee and C. L. Cox, "Vasoactive intestinal peptide selectively depolarizes thalamic relay neurons and attenuates intrathalamic rhythmic activity," *Journal of Neurophysiology*, vol. 90, no. 2, pp. 1224–34, 2003.

[4] E. M. Izhikevich, *Dynamical systems in neuroscience: the geometry of excitability and bursting*, ser. Computational Neuroscience. Cambridge, MA: MIT Press, 2007.

[5] S. Coombes and P. C. Bressloff, Eds., *Bursting: the Genesis of Rhythm in the Nervous System*. World Scientific Publishing Co. Pte. Ltd., 2005.

[6] P. Danzl and J. Moehlis, "Spike timing control of oscillatory neuron models using impulsive and quasi-impulsive charge-balanced inputs," in *Proceddings of the 2008 American Control Conference*, 2008, pp. 171–176.

[7] D. Golomb, X. J. Wang, and J. Rinzel, "Propagation of spindle waves in a thalamic slice model," *J Neurophysiol*, vol. 75, no. 2, pp. 750–769, 1996. [Online]. Available: http://jn.physiology.org/cgi/content/abstract/75/2/750

[8] X.-J. Wang, "Multiple dynamical modes of thalamic relay neurons: rhythmic bursting and intermittent phase-locking," *Neuroscience*, vol. 59, no. 1, pp. 21–31, mar 1994.

[9] G. D. Smith, C. L. Cox, S. M. Sherman, and J. Rinzel, "Fourier analysis of sinusoidally driven thalamocortical relay neurons and a minimal integrate-and-fire-or-burst model," *J Neurophysiol*, vol. 83, no. 1, pp. 588–610, 2000. [Online]. Available: http://jn.physiology.org/cgi/content/abstract/83/1/588

[10] D. McCormick and H. C. Pape, "Properties of a hyperpolarization-activated cation current and its role in rhythmic oscillations in thalamic relay neurons," *J. Physiol.*, vol. 431, pp. 291–318, 1990.

[11] M. Steriade, D. A. McCormick, and T. J. Sejnowski, "Thalamocortical Oscillations in the Sleeping and Aroused Brain," *Science*, vol. 262, pp. 679–685, Oct. 1993.

[12] E. Doedel et. al., "Auto-07p: Continuation and bifurcation software for ordinary differential equations," Tech. Rep., 2008. [Online]. Available: http://sourceforge.net/projects/auto-07p/